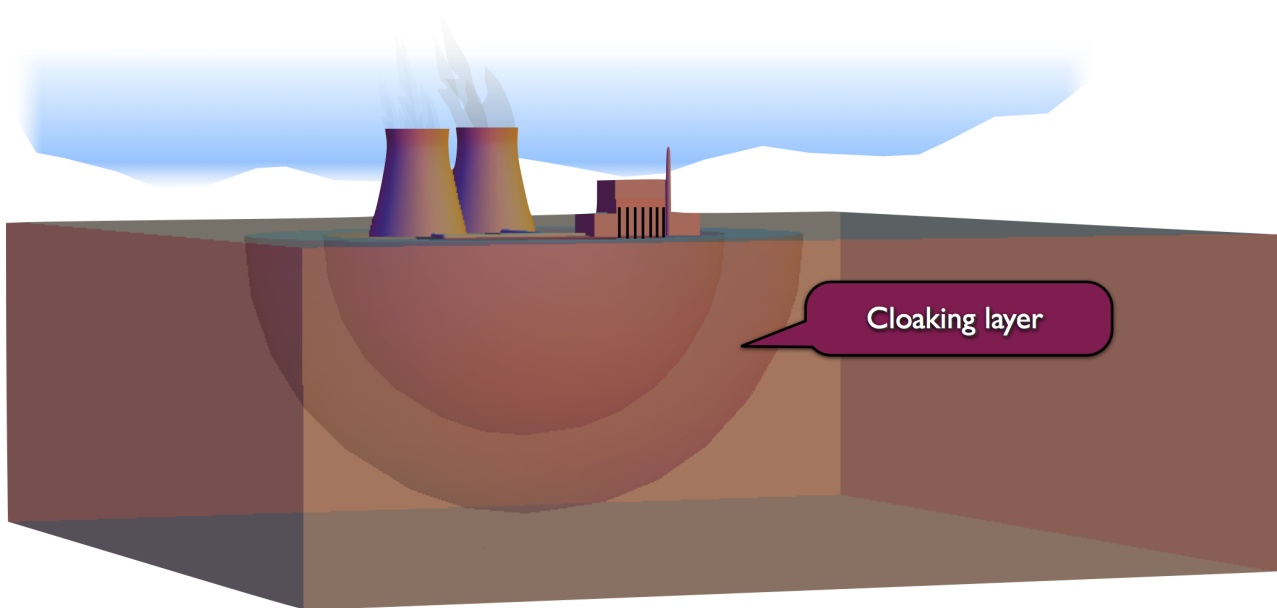


CHALMERS



Designing Materials for Mechanical Invisibility Cloaks

Master's thesis in Solid and Structural Mechanics

ALEXEY KHLOPOTIN
SENAD RAZANICA

Department of Applied Mechanics
Division of Dynamics and Division of Material and Computational Mechanics
CHALMERS UNIVERSITY OF TECHNOLOGY
Gothenburg, Sweden 2012
Master's thesis 2012:50

MASTER'S THESIS IN SOLID AND STRUCTURAL MECHANICS

Designing Materials for Mechanical Invisibility Cloaks

ALEXEY KHLOPOTIN
SENAD RAZANICA

Department of Applied Mechanics
Division of Dynamics and Division of Material and Computational Mechanics
CHALMERS UNIVERSITY OF TECHNOLOGY

Gothenburg, Sweden 2012

Designing Materials for Mechanical Invisibility Cloaks
ALEXEY KHLOPOTIN
SENAD RAZANICA

© ALEXEY KHLOPOTIN, SENAD RAZANICA, 2012

Master's thesis 2012:50
ISSN 1652-8557
Department of Applied Mechanics
Division of Dynamics and Division of Material and Computational Mechanics
Chalmers University of Technology
SE-412 96 Gothenburg
Sweden
Telephone: +46 (0)31-772 1000

Cover:
Potential use of the cloaking material

Chalmers Reproservice
Gothenburg, Sweden 2012

Designing Materials for Mechanical Invisibility Cloaks
Master's thesis in Solid and Structural Mechanics
ALEXEY KHLOPOTIN
SENAD RAZANICA
Department of Applied Mechanics
Division of Dynamics and Division of Material and Computational Mechanics
Chalmers University of Technology

ABSTRACT

Transformation elastodynamics, the solid mechanical counterpart of transformation optics, is an approach to re-routing of mechanical, potentially harmful, transient waves and vibrations, in order to protect sensitive structures or substructures. A large-scale example would be to try to re-route seismic waves, whether from ground explosions or earthquakes, by arranging the properties of the material beneath and around some sensitive infrastructure so as to mimic the surrounding soil without any infrastructure. This can be seen as making the infrastructure "invisible". This term does not refer to making the infrastructure unseen, but rather making it invisible from harmful waves or vibrations. In that case, the effect of the waves acting on the infrastructure will be minimized. A less ambitious (and considerably more realistic) application would be to re-route elastic vibrations around the clamping points of panels in a vehicle, so as to minimize the noise from vibrating panels. Just as for transformation optics, the approach utilizes the concept of form-invariance of the equations of motion under diffeomorphisms to give recipes of how graded materials can mimic homogeneous and isotropic bodies, and cloak the presence of structures within the transformational cloak.

We have studied the use of several types of graded materials for cloaking, and in the present paper we describe how graded micro-polar materials may be used to cloak against Rayleigh waves. We have implemented recipes for the graded properties of a micro-polar cloak from transformation elastodynamics into a modified version of the Structural Mechanics module of COMSOL MultiphysicsTM. In numerical experiments we consider how a modeled, partially buried 'pipeline' may be protected from an incident transient Rayleigh wave by re-routing the wave under the pipeline.

Keywords: Invisibility, Cloak, Meta-materials, Mechanical Invisibility, Homogenization, Micro-polar, Rayleigh waves, Bulk waves

PREFACE

The work presented in this thesis was carried out during 2012 at the Department of Applied Mechanics at Chalmers University of Technology. The thesis was a cross-divisional master thesis with the divisions of Dynamics and Material and Computational Mechanics involved.

ACKNOWLEDGEMENTS

We would like to thank our supervisors, Professor Peter Olsson at department of Dynamics and Docent Fredrik Larsson at department of Material and Computational Mechanics at Chalmers University of Technology, for all the help and support during the thesis work. Alexey would like to thank Senad and Senad would like to thank Alexey!

CONTENTS

Abstract	i
Preface	iii
Acknowledgements	iii
Contents	v
1 Introduction	1
1.1 Purpose	2
1.2 Limitations	2
2 Modeling of meta-materials	3
2.1 Preliminaries	3
2.2 Homogenization	3
2.2.1 Computational Homogenization	4
2.2.2 First order homogenization	4
2.2.3 Second order homogenization	7
2.3 Micro-polar continuum	8
3 Mechanical cloaking of structures	10
3.1 Cloaking transformation	10
3.2 Special case of cloaking transformation for bulk waves	11
4 FE- implementation	13
4.1 Finite Element Method Theory	13
4.1.1 Strong form	13
4.1.2 Weak form	13
4.1.3 FE-formulation	13
4.2 Implementation in COMSOL Multiphysics TM	14
4.2.1 Modifications to COMSOL Multiphysics TM	15
5 Results	17
5.1 Special case - Verification for bulk waves	17
5.2 Considered case - Cloaking for surface waves	19
5.2.1 Geometry	19
5.2.2 Mesh	20
5.2.3 Simulation results	20
6 Discussion	22
7 Conclusions	23

1 Introduction

Less than a decade ago, it was discovered that invisibility cloaking devices could be more than mere fiction. Originally for a type of ‘X-ray’ technique called electric surface impedance tomography, where a voltage distribution is applied to the surface of a body. The resulting electric currents through the surface are then measured, with a view to reconstructing the conductivity inside the object. Theoretically, the interior of the object could, under certain circumstances, hide (or ‘cloak’) an embedded body in such a manner that even the fact that something was hidden would be undetectable. Soon similar phenomena were shown to be possible also for electromagnetic waves.

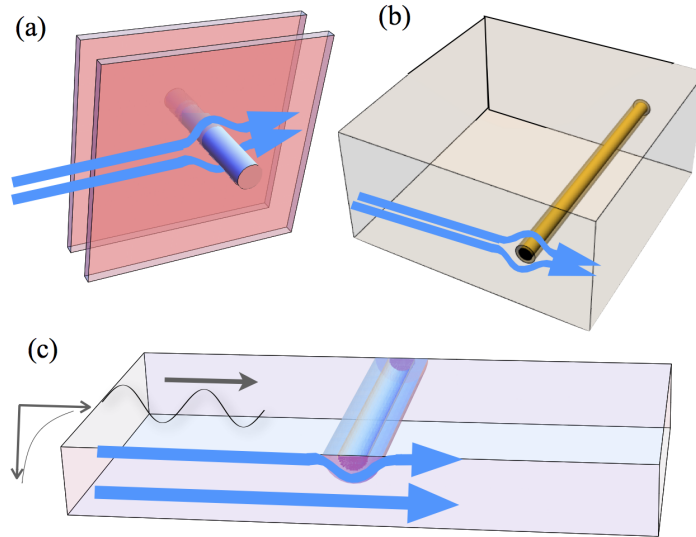


Figure 1.1: *Some geometries where mechanical cloaking might be desirable.*

Also in solid mechanics, there is considerable interest in achieving ‘invisibility,’ however not primarily for hiding objects from sight. Important contributions to elastodynamic transformational cloaking have been given by, among others [16][14][3][8][13]. Recently, an approach to partial cloaking using fiber composites has been explored, see *e.g* [15]. The applications in mechanics include protection of structures and parts of structures from potentially harmful, transient waves and steady state vibrations, see Figure 1.1 for some generic examples. Another, similar type of situation would be ground waves from trains or other vehicles in rapid transit. These waves could possibly be redirected so as to protect buildings situated too close to the tracks or roads. A suggested larger scale application, protection against seismic waves from earthquakes, could be achieved by using cloaking to re-route the waves around sensitive infrastructure, *cf.* Figure 1.2. The cost of a large scale application for protection of for example a nuclear power plant would be astronomical, but it should be compared to the likewise astronomical cost in case of a large-scale collapse of a nuclear power plant due to seismic waves.

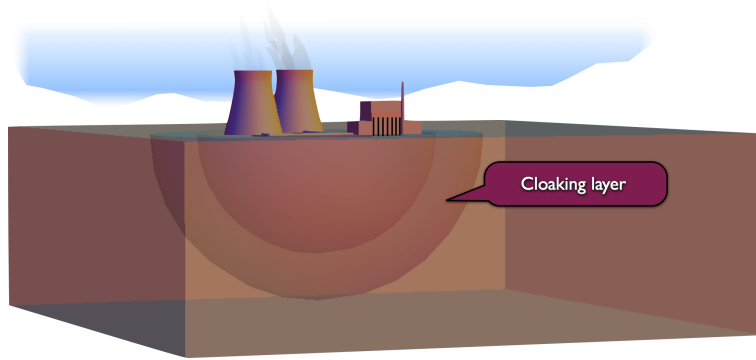


Figure 1.2: *A potential application of mechanical cloaking.*

At smaller scales, an application could be to re-direct elastic waves around e.g. clamping points for panels in vehicles or other structures, thereby achieving some noise control by entirely passive means. On the very small scale, protection of sensitive electronic components from vibrations might be accomplished by surrounding the components by a suitable mechanical cloak. The construction of mechanical cloaks requires fine-tuning of the elastic properties of the cloaking material, so-called meta-materials [1].

Multiscale mechanics is the topic of connecting different length scales in mechanics. For solid materials, the macroscale response is defined through suitable microscale models that resolve the actual topology on the lower scale. The straight-forward question in multiscale mechanics (or micromechanics) is what the macroscale response will be for a given structure on the microscale. One classical example is homogenization of elastic properties for micro-heterogeneous materials [12]. Modern approaches in computational homogenization [9] can also be used to design the microstructure such that a specific response on the macroscale is obtained. In this thesis the results on simulations of cloaking in solid mechanics are described. COMSOL MultiphysicsTM has been used to simulate different material responses. In order to apply the non-symmetric elasticity matrix properties that was needed, a modification of the weak formulation in the software was made. In the next step, simulations of homogenization are required of micro-heterogeneous materials to find meta-materials suitable for producing the required macro-properties for cloaking.

1.1 Purpose

The purpose of this project was to study a few applications of mechanical cloaking using numerical implementation (FEM). In particular, the possibility to construct microstructures that return the required macroscale response, and thus the effective cloaking, was investigated. The analysis was carried out for academic test problems, indicating future possibilities and allowing for rigorous comparison to results in the literature. The study was initially restricted to stationary response and then expanded to transient studies. The goal of the project was to investigate different material models and the possibility to apply these for protection of structures and parts of structures from potentially harmful transient waves and steady state vibrations, which was reported October 2012.

1.2 Limitations

The focus of the project have been on testing one of many transformations from a homogenous media into an anisotropic (cloaking) material. Homogenization of the material should only be made if the investigation concludes that the material can be homogenized using first- and second-order computational homogenization. The simulation was performed on a 2D case and the expansion to 3D case is outside the scope of the thesis. The possibility to design the pertinent meta-material is investigated, however the actual design of topology and properties is outside the the scope of this thesis.

2 Modeling of meta-materials

2.1 Preliminaries

Meta-materials are artificial materials that are designed to have properties that are not found in nature. The properties for these materials are not dominated by the individual atoms rather by artificially produced structures (or "meta-atoms"). In order to model a meta-material, specific material properties are needed in order to produce requested results. This information can be obtained by use of homogenization. Material properties in microscopic scale are studied and RVE:s (Representative volume element) are used to generate effective properties on macroscopic scale. In order to illustrate the procedure, an overview of the computational homogenization model is described in which both first and second order computational homogenization are discussed. Further, micro-polar material is used as cloaking material and micro-polar continuum is described in a general sense.

2.2 Homogenization

Multi-scale modeling is a technique used when solving a problem on two or more scales. On the macro-scale one may have a material that appears isotropic, while being anisotropic/heterogeneous on its micro-scale. In order to obtain the effective properties on macro-scale, the micro-scale with its RVE is used. Assuming separation of scales these RVEs represent the material properties in single points on the macro-scale. The effective properties of a specific material are obtained by use of volume averaging, or homogenization, on a computational cell with typical diameter L_{\square} although the shape of the computational cell is irrelevant in principle. If a random microstructure is considered, the true effective properties are then obtained as the converged values when L_{\square} becomes sufficiently large. In practice it is always necessary to choose a cell of finite size, an RVE, with typical diameter L_{RVE} . The definition of the RVE can be expressed as a statistically representative sample of the considered material on the subscale. See Figure 2.3 for an illustration of a RVE and its deformation.

If complete scale separation is taken into account then in order for it to be qualified as RVE its size L_{RVE} must be,

- Sufficiently small compared to the typical macroscale dimension of the structural component
 $L_{RVE} \ll L^{MAC}$

- Sufficiently large compared to the typical subscale dimension of microconstituents e.g. grains,
 $L_{sub} \ll L_{RVE}$

That the RVE is sufficiently small here means that the primary variables such as, macroscale smooth displacement vary at most linearly within the RVE. This is known as scale separation or first order homogenization. In the other case when RVE is sufficiently large then this indicates that the average field variables for a given microscopic "point" do not change significantly at further increase of the RVE size.

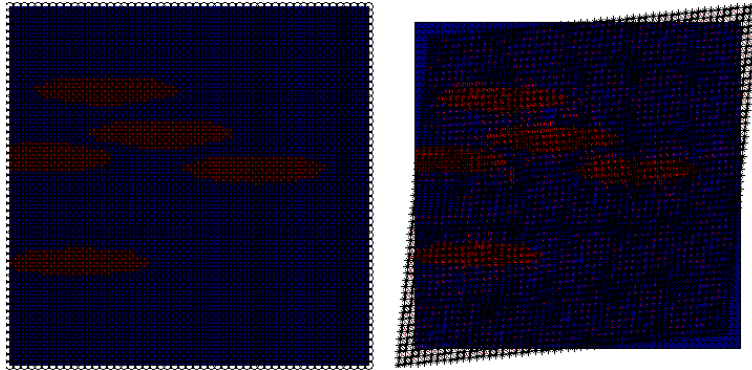


Figure 2.1: *Undeformed and deformed RVE example*

2.2.1 Computational Homogenization

First, an RVE is assigned to each integration point on macro-scale. Boundary conditions are then applied on the RVE in order to calculate the stiffness. There are different boundary conditions that can be applied on the RVE; displacements boundary conditions (DBC), traction boundary condition (TBC) and periodic boundary conditions (PBC). Solving the boundary value problem gives the consistent constitutive tangent stiffness, \mathbf{C} , which can be calculated for each element of the RVE. Using the volume averaging from homogenization, the effective properties can be calculated and returned to macro-scale integration point. These are then used to assemble the macro stiffness and to solve the problem[9]. See Figure 2.2 for the procedure of first order computational homogenization.

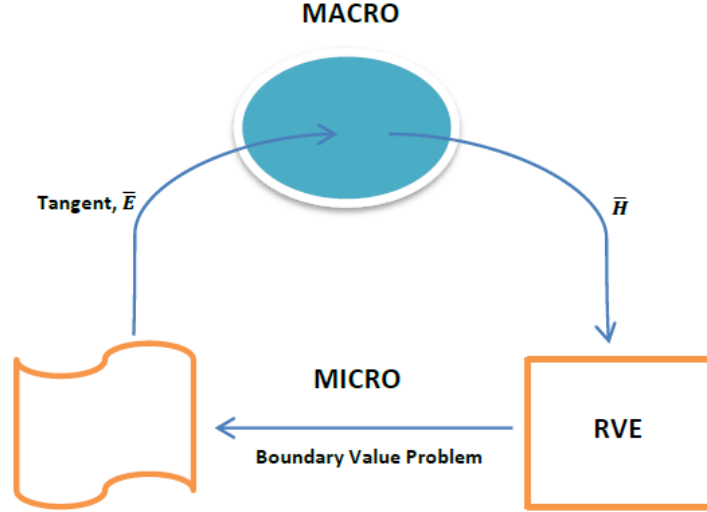


Figure 2.2: *First-Order Computational Homogenization Scheme.*

2.2.2 First order homogenization

Static equilibrium equation

$$-\nabla \cdot \boldsymbol{\sigma}^T = \mathbf{f} \quad \text{in } \Omega_{\square} \quad (2.2.1)$$

The volume averages on the RVE can be defined as

$$\langle \square \rangle \stackrel{def}{=} \frac{1}{|\Omega_{\square}|} \int_{\Omega_{\square}} \square d\Omega$$

Introducing the effective strain and stress tensors as the averages yields

$$\bar{\boldsymbol{\varepsilon}} \stackrel{def}{=} \langle \boldsymbol{\varepsilon} \rangle_{\square}, \quad \bar{\boldsymbol{\sigma}} \stackrel{def}{=} \langle \boldsymbol{\sigma} \rangle_{\square}$$

From now on the strain tensor is denoted as, $\boldsymbol{\varepsilon} = \nabla \otimes \mathbf{u}$. By use of the Gauss Theorem it is possible to transform the volume integrals from the strain and stress averages to surface integrals on the RVE [5].

From the strain and stress averages we make use of the Gauss Theorem to obtain the identity

$$\int_{\Omega_{\square}} \nabla \otimes \mathbf{u} \, d\Omega = \int_{\Gamma_{\square}} \mathbf{u} \otimes \mathbf{n} \, d\Gamma \quad (2.2.2)$$

Here, \mathbf{n} is the outward unit normal on Γ_{\square} . This then gives that

$$\langle \boldsymbol{\varepsilon} \rangle_{\square} = \frac{1}{|\Omega_{\square}|} \int_{\Omega_{\square}} \boldsymbol{\varepsilon} \, d\Omega = \frac{1}{2|\Omega_{\square}|} \int_{\Omega_{\square}} [\nabla \otimes \mathbf{u} + [\nabla \otimes \mathbf{u}]^T] \, d\Omega = \frac{1}{2|\Omega_{\square}|} \int_{\Gamma_{\square}} [\mathbf{u} \otimes \mathbf{n} + [\mathbf{u} \otimes \mathbf{n}]^T] \, d\Gamma \quad (2.2.3)$$

$$\begin{aligned}
\langle \boldsymbol{\sigma} \rangle_{\square} &= \frac{1}{|\Omega_{\square}|} \int_{\Omega_{\square}} \boldsymbol{\sigma} \, d\Omega = \frac{1}{|\Omega_{\square}|} \int_{\Omega_{\square}} \boldsymbol{\nabla} \cdot [\boldsymbol{\sigma}^{\top} \otimes \mathbf{x}] \, d\Omega + \frac{1}{|\Omega_{\square}|} \int_{\Omega_{\square}} \mathbf{f} \otimes \mathbf{x} \, d\Omega = \\
&= \frac{1}{|\Omega_{\square}|} \int_{\Gamma_{\square}} \mathbf{n} \cdot \boldsymbol{\sigma}^{\top} \otimes \mathbf{x} \, d\Gamma + \frac{1}{|\Omega_{\square}|} \int_{\Omega_{\square}} \mathbf{f} \otimes \mathbf{x} \, d\Omega
\end{aligned} \tag{2.2.4}$$

In the special case when $\mathbf{f} = \mathbf{0}$

$$\langle \boldsymbol{\sigma} \rangle_{\square} = \frac{1}{|\Omega_{\square}|} \int_{\Gamma_{\square}} \mathbf{t} \otimes \mathbf{x} \, d\Gamma \tag{2.2.5}$$

In order to connect the macroscopic properties to the microscopic the Hill- Mandel macrohomogeneity condition is used

$$\bar{\boldsymbol{\sigma}} : \delta \bar{\boldsymbol{\varepsilon}} = \langle \boldsymbol{\sigma} : \delta \boldsymbol{\varepsilon} \rangle_{\square} \quad \forall \delta \mathbf{u} \in \mathbf{U}_{\square} \tag{2.2.6}$$

Where \mathbf{U}_{\square} is the space of admissible displacements \mathbf{u} which is restricted to a given RVE occupying the domain Ω_{\square} with the boundary Γ_{\square} .

In the case of linear elasticity on the subscale the effective constitutive relationship is defined as

$$\bar{\boldsymbol{\sigma}} = \mathbf{C} : \bar{\boldsymbol{\varepsilon}} \tag{2.2.7}$$

where \mathbf{C} is the constitutive tangent stiffness. The classical boundary conditions used for the RVE problem in 2.2.1 are the

Displacement boundary conditions (DBC)

$$\mathbf{u}(\mathbf{x}) = \bar{\mathbf{u}} + \bar{\boldsymbol{\varepsilon}} \cdot [\mathbf{x} - \bar{\mathbf{x}}] \quad \mathbf{x} \in \Gamma_{\square} \tag{2.2.8}$$

Which typically gives an overly stiff response for a small RVE.

Traction boundary condition (TBC)

$$\mathbf{t}(\mathbf{x}) = \bar{\boldsymbol{\sigma}} \cdot \mathbf{n} \quad \mathbf{x} \in \Gamma_{\square} \tag{2.2.9}$$

Which typically results in a too low stiffness.

When the size of the RVE increases, the results for (DBC) and (TBC) converges. Periodic boundary conditions (PBC) are more accurate but does not the desired boundary conditions.

Two scale implementation in FEM, FE^2 , for a linear problem

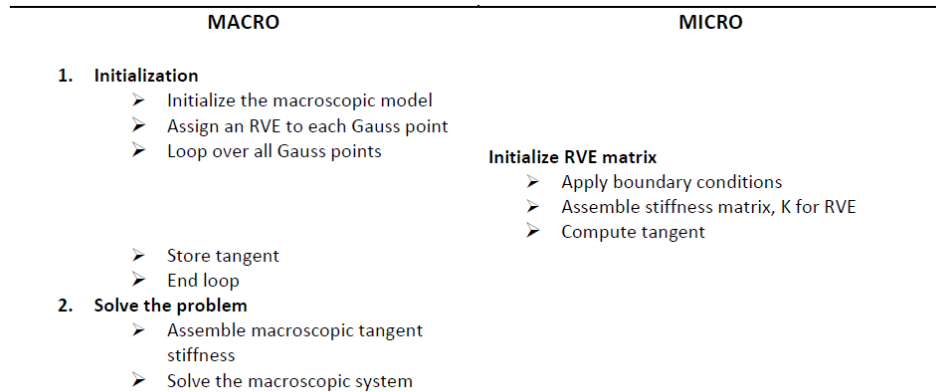


Figure 2.3: *Implementation scheme.*

First a macro mesh is generated for the problem considered. At every integration point a RVE is assigned. Loop over all elements in the macro mesh and for each element a RVE calculation is performed based on the boundary conditions discussed earlier. Using the homogenization theory the averaged material properties can be calculated from the assembled RVE stiffness matrix.

The consistent constitutive tangent stiffness is then computed and returned to every integration point on the macro mesh. Using the tangent, the stiffness matrix of the macro scale is computed and used when solving the macroscopic system, see Figure 2.3

Note : If microscopically homogeneous, the tangent will be the same and only one RVE has to be calculated.

2.2.3 Second order homogenization

Previously the first order computational homogenization has been presented. This method has two major disadvantages; first, the method does not incorporate the size of the microstructure analyzed which makes it impossible to address geometrical size effects that can occur. Secondly, when it comes to uniformity of the microscopic fields to each microstructural representative cell a difficulty arise. This uniformity relies on scale separation and is not valid in critical regions of high deformation gradients, where a high variation of the microscopic fields is present. In order to solve the mentioned problems, a second order computational homogenization procedure is used. This method leads to a higher order continuum model that uses the macroscopic deformation tensor and its gradient to define the essential boundary conditions on a microstructural RVE. Based on the boundary conditions, the boundary value problem can be solved which generates the macroscopic stress tensor and a higher-order stress tensor. In general this will by automation deliver the microstructurally based constitutive response of the higher order macrocontinuum. Figure 2.4 illustrates the procedure for a second order homogenization scheme.

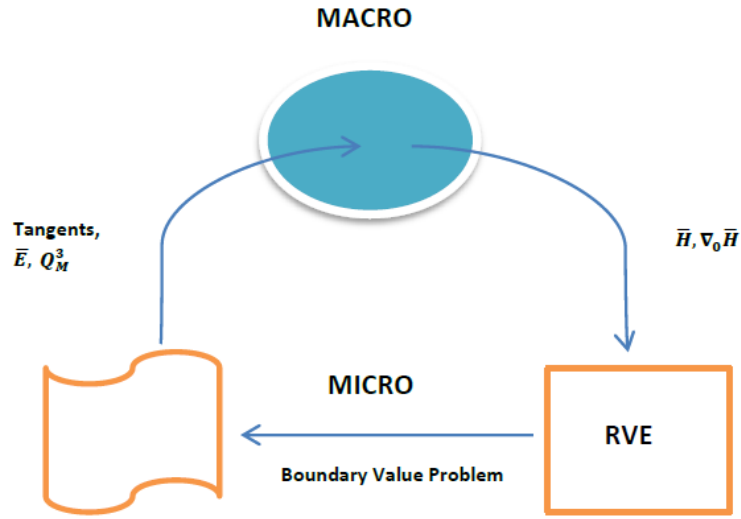


Figure 2.4: *Second-Order Computational Homogenization Scheme.*

Consider an non-linear map that describes the transformation from the undeformed macroscopic state \mathbf{X} , to the deformed state \mathbf{x} at time t . This map can then be described as $\mathbf{x} = \phi(\mathbf{X}, t)$. For an infinitesimal element, classical continuum mechanics lead to the linear mapping

$$d\mathbf{x} = \frac{\partial \phi}{\partial \mathbf{X}} \cdot d\mathbf{X} = \mathbf{H} \cdot d\mathbf{X} \quad (2.2.10)$$

The deformation gradient tensor \mathbf{H} is given by

$$\mathbf{H} = \left(\frac{\partial \phi}{\partial \mathbf{X}} \right) = (\nabla \mathbf{x}) = \overline{\nabla \otimes \nabla \otimes \mathbf{u}} \quad (2.2.11)$$

The equations 2.2.11 can be used as point of departure from the first-order computational homogenization. When line elements in volumes of finite size are involved, the computations become more complicated due to the fact that equation 2.2.11 is not applicable in this case. Therefore a new expression for $\Delta \vec{x}$ might be obtained as

$$\Delta \mathbf{x} = \mathbf{H} \cdot \Delta \mathbf{X} + \frac{1}{2} \Delta \mathbf{X} \cdot \nabla \mathbf{G} \cdot \Delta \mathbf{X} + O(\Delta \mathbf{X}^3) \quad (2.2.12)$$

where \mathbf{G} is a third order tensor and computed as

$$\mathbf{G} = \frac{\partial}{\partial \mathbf{X}} \left(\frac{\partial \phi}{\partial \mathbf{X}} \right) = \nabla \mathbf{H} \quad (2.2.13)$$

For the second order computational homogenization approach both the macroscopic deformation tensor \mathbf{H} , and its gradient \mathbf{G} are used to prescribe the kinematic boundary conditions on an RVE. The equilibrium equation for the microstructural RVE (in the absence of body forces) is defined as

$$\nabla \cdot \boldsymbol{\sigma}^T = \mathbf{0} \quad (2.2.14)$$

where $\boldsymbol{\sigma}^T$ is the Cauchy stress tensor. To be able to determine the RVE averaged stress measures an extension of the Hill-Mandel condition is used as

$$\frac{1}{V_0} \int_{V_0} \boldsymbol{\sigma} : \delta \mathbf{H} dV_0 = \boldsymbol{\sigma} : \delta \mathbf{H} + \mathbf{Q} : \delta \mathbf{G} \quad (2.2.15)$$

here \mathbf{Q} is the macroscopic higher order stress tensor. The relations for $\boldsymbol{\sigma}$ and \mathbf{Q} are

$$\boldsymbol{\sigma} = \frac{1}{V_0} \int_{\Gamma_0} \mathbf{p} \mathbf{X} d\Gamma_0 \quad (2.2.16)$$

$$\mathbf{Q} = \frac{1}{2V_0} \int_{\Gamma_0} \mathbf{X} \mathbf{p} \mathbf{X} d\Gamma_0 \quad (2.2.17)$$

These equations relate the macroscopic stress tensor and the macroscopic higher order stress tensor to microstructural variables on the RVE boundary. Here the higher order model on the macroscale is defined as

$$-\nabla \cdot \boldsymbol{\sigma}^T + \nabla \cdot (\nabla \cdot \mathbf{Q})^T = \mathbf{0} \quad (2.2.18)$$

2.3 Micro-polar continuum

Another empiric model accounting for size effects is the micro-polar continuum. When classical continuum mechanics is considered then each material particle is assigned a certain position, irrespective of orientation, at a certain time. The difference between these materials and micro-polar materials is that, micro-polar material can additionally be oriented. In order to define the orientation of the micro-polar material an additional object is assigned, called "director". Micro-polar continuum can be viewed as a special case of micromorphic continuum. This means that micromorphic materials undergo an additional micromotion in comparison to classical continuum mechanics. This additional micromotion corresponds to the rotation and deformation of the material particle at microscale. This micromotion is the "director" and is denoted by ϕ [17].

Considering the stress tensor of micro-polar continuum mechanics then it is noted that this tensor is no longer symmetric which is a result of the independent spin of particles. In order to derive the balance laws of mechanics and the constitutive equations needed for a broad arsenal of micro-polar materials, axiomatic methods of rotational mechanics or continuum mechanics as well as methods for invariant quantity and of functional analysis are taken into consideration.

In the beginning of this chapter the governing and constitutive equations for the case considered are described. In order to use a material that has the possibility to cloak or deflect vibrations of different kinds, a specific configurations has to be fulfilled. The constitutive stiffness matrix \mathbf{C} has to have major symmetry but not minor symmetry. Therefore one of the materials that satisfies the needed configuration is micro-polar material. This leads to some difficulties regarding computational homogenization. Both first and second order computational homogenization requires not only major symmetry but also minor symmetry. This indicates that neither of these can be used in order to model the material of interest. Therefore other evaluation techniques have to be used. A study on the relation between second order homogenization and micro-polar theory is presented in [6]. A general (hemitropic) micro-polar medium satisfies the constitutive equations[18][4]

$$\boldsymbol{\sigma} = \mathbf{C} : (\nabla \otimes \mathbf{u} - \boldsymbol{\epsilon} \cdot \boldsymbol{\phi}) + \mathbf{B} : (\nabla \otimes \boldsymbol{\phi}) \quad (2.3.1)$$

$$\boldsymbol{\mu} = \mathbf{B}^T : (\nabla \otimes \mathbf{u} - \boldsymbol{\epsilon} \cdot \boldsymbol{\phi}) + \mathbf{A} : (\nabla \otimes \boldsymbol{\phi}) \quad (2.3.2)$$

and the equations of motion

$$\nabla \cdot \boldsymbol{\sigma}^T = \rho \ddot{\mathbf{u}} \quad (2.3.3)$$

$$\nabla \cdot \boldsymbol{\mu}^T + \boldsymbol{\epsilon} : \boldsymbol{\sigma} = \mathbf{J} \cdot \ddot{\boldsymbol{\phi}} \quad (2.3.4)$$

The totally non-symmetric third order tensor in three dimensions may be defined as $\boldsymbol{\epsilon} = \mathbf{I} \times \mathbf{I}$, where \mathbf{I} is the second order unit tensor. The double contraction is defined so that $\mathbf{X} : \mathbf{Y} = X_{ij} Y_{ij}$ for $\mathbf{X} = X_{ij} \mathbf{e}_i \otimes \mathbf{e}_j$ and

$\mathbf{Y} = Y_{ij}\mathbf{e}_i \otimes \mathbf{e}_j$. Similarly $\mathbf{K} : \mathbf{Y} = K_{ijkl}Y_{kl}\mathbf{e}_i \otimes \mathbf{e}_j$ for $\mathbf{K} = K_{ijkl}\mathbf{e}_i \otimes \mathbf{e}_j \otimes \mathbf{e}_k \otimes \mathbf{e}_l$. \mathbf{C} , \mathbf{A} are major symmetric tensors of order 4. The symmetry is under transpose of the first and last index *pairs*. Boldface superscript \mathbf{T} has been used to denote this transposition, and ordinary sans serif \mathbf{T} for transpose of second-order tensors. The major symmetry requirement can thus be stated as

$$\begin{aligned}\mathbf{A}^{\mathbf{T}} &= A_{klij}\mathbf{e}_i \otimes \mathbf{e}_j \otimes \mathbf{e}_k \otimes \mathbf{e}_l \\ &= A_{ijkl}\mathbf{e}_i \otimes \mathbf{e}_j \otimes \mathbf{e}_k \otimes \mathbf{e}_l = \mathbf{A}\end{aligned}$$

and similarly for \mathbf{C} . Note that neither of these tensors need satisfy the minor symmetries, whereby *e.g.* $C_{ijkl} \neq C_{ijlk}$ in general. \mathbf{B} is a tensor of order 4, with no assumptions on symmetry. Computational homogenization for micro-polar material continuum has been proposed by [6] where an energy equivalent RVE was considered. However, the consistent kinematic description is still an open question.

We now assume three things. First, that the material is centro-symmetric so that $\mathbf{B} = \mathbf{0}$. Second, that time-harmonic conditions prevail, with time factor $\exp(-i\omega t)$. And third, that the curvature stiffness is much higher than the stiffness with respect to strains. Then the tensor \mathbf{A} in some suitable sense becomes very large, while the micro-moment tensor $\boldsymbol{\mu}$ remains finite.

To be slightly more specific regarding the last point, let's say that we *e.g.* have some scalar parameter a that we let tend to positive infinity, and that for some $\epsilon > 0$

$$\mathbf{A} = a\mathbf{M} \boxtimes \mathbf{M} + \mathcal{O}[a^{1-\epsilon}] \quad \text{as } a \rightarrow +\infty$$

where $\mathbf{M} = M_{ij}\mathbf{e}_i \otimes \mathbf{e}_j$ is some second order tensor. (We also assume that the matrix formed from its coefficients M_{ij} is invertible.) Here the boxed multiplication of two second order tensors is defined as

$$\mathbf{X} \boxtimes \mathbf{Y} = X_{ik}Y_{jl}\mathbf{e}_i \otimes \mathbf{e}_j \otimes \mathbf{e}_k \otimes \mathbf{e}_l$$

Then, if $\boldsymbol{\mu}$ is to remain finite, we must have that $\nabla \otimes \boldsymbol{\phi} \rightarrow \mathbf{0}$ as $a \rightarrow +\infty$, and $\boldsymbol{\phi} \rightarrow \text{constant}$ throughout the body. If the boundary condition is $\boldsymbol{\phi}|_{\partial\Omega} = \mathbf{0}$, and the limit of $\boldsymbol{\phi}$ is uniform, then in the limit $\boldsymbol{\phi}$ must vanish throughout Ω .

Under these three assumptions, the set of four equations implies

$$\nabla \cdot \boldsymbol{\sigma}^{\mathbf{T}} + \rho\omega^2 \mathbf{u} = \mathbf{0} \quad \text{in } \Omega \quad (2.3.5)$$

$$\boldsymbol{\sigma} = \mathbf{C} : (\nabla \otimes \mathbf{u}) \quad (2.3.6)$$

This means that, given suitable boundary conditions on the displacement and/or traction vector, the assumption leads to gives a boundary value problem for the displacement field alone. The field $\boldsymbol{\mu}$ may subsequently be retrieved. Equations 2.3.5 and 2.3.6, must be supplemented by a boundary condition

$$\hat{\mathbf{n}} \cdot \boldsymbol{\sigma}^{\mathbf{T}}|_{\partial\Omega} = \mathbf{h} \quad (2.3.7)$$

where \mathbf{h} is a prescribed vector field defined on $\partial\Omega$, and $\hat{\mathbf{n}}$ is the outward-pointing unit normal.

3 Mechanical cloaking of structures

3.1 Cloaking transformation

As found in a special case in [7], and more generally in [13], a body consisting of this kind of micro-polar material can mimic a homogeneous isotropic elastic body in the following sense: If the body inside Ω is micro-polar with a stiffness and density that varies in a suitable manner, the Traction-to-Displacement (TtD) map, that maps $\mathbf{h} \mapsto \mathbf{u}|_{\partial\Omega}$ for the micro-polar solid, may be identically the same as that of a homogeneous, isotropic solid occupying the same region Ω .

Consider a diffeomorphism $\psi : \Omega \rightarrow \Omega$ such that the limit of ψ on $\partial\Omega$ is the identity map. Let $\mathbf{C} = C_{ijkl} \mathbf{e}_i \otimes \mathbf{e}_j \otimes \mathbf{e}_k \otimes \mathbf{e}_l$ denote the elasticity tensor a homogeneous isotropic elastic material, and let ρ_0 be its constant mass density, and put

$$\begin{aligned} C_{ijkl}(\mathbf{X}) &= J(\mathbf{X}) \frac{\partial X^j}{\partial x^p} c_{ipkq} \frac{\partial X^l}{\partial x^q} \\ \rho(\mathbf{X}) &= J(\mathbf{X}) \rho_0 \end{aligned} \tag{3.1.1}$$

where

$$\mathbf{x} = \psi(\mathbf{X}), \quad J(\mathbf{X}) = \det\left(\frac{\partial\psi(\mathbf{X})}{\partial\mathbf{X}}\right), \quad \frac{\partial\mathbf{X}}{\partial\mathbf{x}} = \left(\frac{\partial\psi(\mathbf{X})}{\partial\mathbf{X}}\right)^{-1}$$

Note that the elasticity tensor of the micro-polar material, with components given by Eq. (3.1.1), does indeed satisfy the major symmetry condition. Then we may consider the x^j as cartesian coordinates in the homogeneous isotropic solid, and the X^j as cartesian coordinates in the inhomogeneous, anisotropic micro-polar material, each occupying Ω . If the displacement field in the homogeneous material is $\mathbf{u}(\mathbf{x})$, satisfying

$$\frac{\partial}{\partial x^j} \left(c_{ijpq} \frac{\partial u_p(\mathbf{x})}{\partial x^q} \right) + \rho_0 \omega^2 u_i(\mathbf{x}) = 0 \tag{3.1.2}$$

then $\mathbf{U}(\mathbf{X}) = \mathbf{u}(\psi^{-1}(\mathbf{X}))$ satisfies

$$\frac{\partial}{\partial X^j} \left(C_{ijpq}(\mathbf{X}) \frac{\partial U_p(\mathbf{X})}{\partial X^q} \right) + \rho(\mathbf{X}) \omega^2 U_i(\mathbf{X}) = 0 \tag{3.1.3}$$

Even without special assumptions on the normal derivative of ψ on $\partial\Omega$, it may be verified that both tractions and displacements on the boundary $\partial\Omega$ coincide in the two cases. For any surface excitation of the micro-polar body, the response at the boundary is the same as for a homogeneous body. The TtD maps of the two bodies are identical.

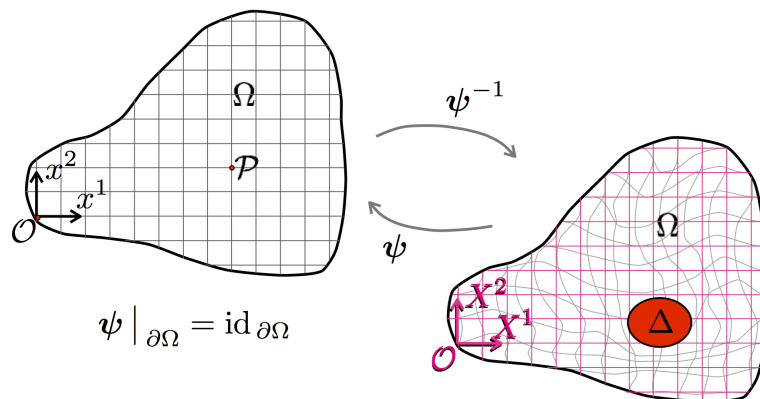


Figure 3.1: ‘Blowing up’ a point to make a hiding-place.

The idea is by blowing up a point in the homogeneous material model into the anisotropic (cloaking) material model by means of the transformation, one can then hide an object inside the new domain, see Figure 3.1. The cloak is primarily constructed for bulk waves, but also works well with Rayleigh waves. This because the Rayleigh wave effects are isolated to the surface and will thus mimic bulk waves and the boundary conditions on the surface will be satisfied because of symmetry [11].

3.2 Special case of cloaking transformation for bulk waves

One possible transformation can be found in literature by Brun et al. [7]. The transformation used is illustrated in Figure 3.1

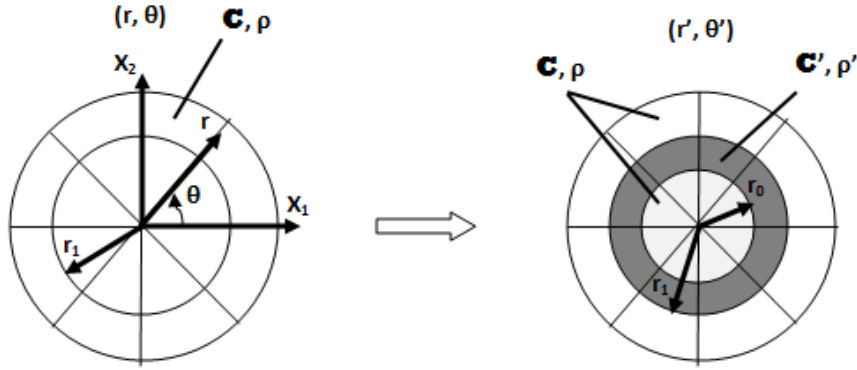


Figure 3.1: *Brun transformation*

Coordinate transformation

$$\begin{aligned} r' &= r_0 + \frac{r_1 - r_0}{r_1} r, & \theta' &= \theta & \text{if } r &\leq r_1 \\ r' &= r, & \theta' &= \theta & \text{if } r &> r_1 \end{aligned}$$

Outside the cloak ($r > r_1$) and inside the cloak ($r < r_0$) we have (Navier equation):

$$\nabla \cdot \mathbf{C} : \nabla \mathbf{u} + \rho \omega^2 \mathbf{u} + \mathbf{b} = \mathbf{0}$$

where \mathbf{u} is the displacement, ρ is density, \mathbf{C} is the fourth-order constitutive tensor of linear elastic material and $\mathbf{b} = \mathbf{b}(\mathbf{x})$ is the spatial distribution of a simple harmonic force.

After the transformation, in the region $r' \in [r_0, r_1]$ the Navier equations are mapped into equations:

$$\nabla \cdot \mathbf{C}' : \nabla \mathbf{u} + \rho' \omega^2 \mathbf{u} = \mathbf{0}$$

where the body forces are outside the ring and the stretched density is:

$$\rho' = \frac{r - r_0}{r} \left(\frac{r_1}{r_1 - r_0} \right)^2 \rho$$

and the elasticity tensor \mathbf{C}' has non zero cylindrical components:

$$\begin{aligned} C'_{rrrr} &= \frac{r - r_0}{r} (\lambda + 2\mu), & C'_{\theta\theta\theta\theta} &= \frac{r}{r - r_0} (\lambda + 2\mu), \\ C'_{rr\theta\theta} &= C'_{\theta\theta rr} = \lambda, & C'_{r\theta\theta r} &= C'_{\theta r r \theta} = \mu, \end{aligned}$$

$$C'_{r\theta r\theta} = \frac{r-r_0}{r}\mu, \quad C'_{\theta r\theta r} = \frac{r}{r-r_0}\mu$$

with λ and μ the Lamé moduli characterizing the isotropic behavior described by \mathbf{C} . \mathbf{C}' has not the minor symmetries.

At the outer boundary of the cloak ($r = r_1$), the transformation gives $r' = r_1$. The transformed density on this boundary is:

$$\rho' = \frac{r_1}{r_1 - r_0}\rho$$

and the transformed cylindrical components of the elasticity tensor are:

$$C'_{rrrr} = \frac{r_1 - r_0}{r_1}(\lambda + 2\mu), \quad C'_{r\theta r\theta} = \frac{r_1 - r_0}{r_1}\mu$$

This transformation has been tested to verify the implementation in the software and the results can be found in Chapter 5.

4 FE- implementation

4.1 Finite Element Method Theory

To implement and test our transformation a model can be implemented using FEM. There are a lot of software that are based on this theory and COMSOL MultiphysicsTM is one of them. With this theory one can implement the model in MATLAB, but the calculation speed may be slow.

4.1.1 Strong form

The equation of motion is stated as (stationary):

$$\nabla \cdot [\mathbf{C} : (\nabla \otimes \mathbf{u})]^\top + \rho \omega^2 \mathbf{u} + \mathbf{b} = \mathbf{0} \quad (4.1.1)$$

which can be written as:

$$\nabla \cdot \boldsymbol{\sigma}^\top + \rho \omega^2 \mathbf{u} + \mathbf{b}(t) = \mathbf{0} \quad (4.1.2)$$

4.1.2 Weak form

Using a weight vector \mathbf{v} and multiplying it on both sides of the equation gives:

$$\int_{\mathbf{A}} \mathbf{v}^\top (\nabla \cdot \boldsymbol{\sigma}^\top + \rho \omega^2 \mathbf{u} + \mathbf{b}) \, dA = 0 \quad (4.1.3)$$

Using that (Gauss theorem):

$$\int_{\mathbf{A}} \mathbf{v}^\top (\nabla \cdot \boldsymbol{\sigma}^\top) \, dA = \int_{\Gamma_h} \mathbf{v}^\top \mathbf{h} \, d\Gamma + \int_{\Gamma_g} \mathbf{v}^\top \mathbf{t} \, d\Gamma - \int_{\mathbf{A}} (\nabla \mathbf{v})^\top \boldsymbol{\sigma} \, dA$$

We get

$$\int_{\mathbf{A}} \mathbf{v}^\top (\nabla \cdot \boldsymbol{\sigma}^\top) \, dA - \int_{\mathbf{A}} \mathbf{v}^\top \rho \omega^2 \mathbf{u} \, dA = \int_{\Gamma_h} \mathbf{v}^\top \mathbf{h} \, d\Gamma + \int_{\Gamma_g} \mathbf{v}^\top \mathbf{t} \, d\Gamma + \int_{\mathbf{A}} \mathbf{v}^\top \mathbf{b}(t) \, dA \quad \text{for } t \in (0, T) \quad (4.1.4)$$

$$\mathbf{u} = \mathbf{g}(t) \text{ on } \Gamma_g, t \in (0, T)$$

$$\mathbf{u} = \mathbf{u}_0 \text{ in } A, t \in (0, T)$$

$$(\mathbf{u} = \dot{\mathbf{u}}_0 \text{ on } \Gamma_g, t \in (0, T))$$

This is the weak form with boundary conditions, which can be used together with Galerkins method in order to implement this in FEM.

4.1.3 FE-formulation

Hooke's elasticity:

$$\boldsymbol{\sigma} = \mathbf{C} : (\nabla \otimes \mathbf{u}) \quad (4.1.5)$$

With Galerkin method one can convert the continuous problem into a discrete problem which can then be implemented in the computer. Using Galerkin method we approximate \mathbf{u} as $\mathbf{u} = \mathbf{N}\mathbf{a}$ and inserting into the weak form yields:

$$-\omega^2 \mathbf{M}\mathbf{a} + \mathbf{K}\mathbf{a} = \mathbf{f} \quad (4.1.6)$$

where

$$(\mathbf{K})_{ij} = \int_{\mathbf{A}} (\nabla \otimes \mathbf{N}_i) : \mathbf{C} : (\nabla \otimes \mathbf{N}_j) \, dA$$

$$(M)_{ij} = \int_{\mathbf{A}} \mathbf{N}_i \rho \mathbf{N}_j dA$$

$$\mathbf{f} = \int_{\Gamma_h} \mathbf{N}^T \mathbf{h} d\Gamma + \int_{\Gamma_g} \mathbf{N}^T \mathbf{t} d\Gamma + \int_{\mathbf{A}} \mathbf{N}^T \mathbf{b}(t) dA$$

The final equations for the stationary problem can be written as:

$$(\mathbf{K} - \omega^2 \mathbf{M}) \mathbf{a} = \mathbf{f} \quad (4.1.7)$$

In order to model a transient problem we have the equation of motion as:

$$\nabla \boldsymbol{\sigma} + \rho \omega^2 \ddot{\mathbf{u}} + \mathbf{b}(t) = \mathbf{0} \quad (4.1.8)$$

Using the same procedure as before, e.g. obtaining weak form and then strong form, we obtain the final equation:

$$\mathbf{M} \ddot{\mathbf{a}} + \mathbf{K} \mathbf{a} = \mathbf{f} \quad (4.1.9)$$

which is semi-discrete, e.g. discrete in space but not in time.

4.2 Implementation in COMSOL MultiphysicsTM

Name	Expression
r0	0.2 [m]
r1	0.4 [m]
rho0	1 [kg/m ³]
mu0	1 [Pa]
lambda0	2.3 [Pa]
b	1 [N]
nu	lambda0/(2*(lambda0+mu0))
omega	6[rad/s]
ks	omega/(sqrt(mu0/rho0))
As	1[m ²]

Figure 4.1: Parameters used in COMSOL MultiphysicsTM

To implement the considered model into COMSOL MultiphysicsTM, a number of parameters had to be defined, as indicated in Figure 4.1. With these values all other important functions and parameters can be constructed and used in the software. The radial values, **r0** and **r1** describe the inner and outer radii of the cloaking region. **ks** and **As** are parameters used for the Rayleigh wave construction in the software while the rest are material parameters that describe the material characteristics.

4.2.1 Modifications to COMSOL Multiphysics™

In the model considered in this thesis, the elasticity matrix is not symmetric as in the standard COMSOL Multiphysics™ Structural Mechanics module. The elasticity matrix in COMSOL Multiphysics™ is represented as in Figure 4.2.

Due to the symmetry, the elasticity tensor can be completely represented by a symmetric 6-by-6 matrix as:

$$D = \begin{bmatrix} D_{11} & D_{12} & D_{13} & D_{14} & D_{15} & D_{16} \\ D_{12} & D_{22} & D_{23} & D_{24} & D_{25} & D_{26} \\ D_{13} & D_{23} & D_{33} & D_{34} & D_{35} & D_{36} \\ D_{14} & D_{24} & D_{34} & D_{44} & D_{45} & D_{46} \\ D_{15} & D_{25} & D_{35} & D_{45} & D_{55} & D_{56} \\ D_{16} & D_{26} & D_{36} & D_{46} & D_{56} & D_{66} \end{bmatrix} = \begin{bmatrix} c^{1111} & c^{1122} & c^{1133} & c^{1112} & c^{1123} & c^{1113} \\ c^{1122} & c^{2222} & c^{2233} & c^{2212} & c^{2223} & c^{2213} \\ c^{1133} & c^{2233} & c^{3333} & c^{3312} & c^{3323} & c^{3313} \\ c^{1112} & c^{2212} & c^{3312} & c^{1212} & c^{1223} & c^{1213} \\ c^{1123} & c^{2223} & c^{3323} & c^{1223} & c^{2323} & c^{2313} \\ c^{1113} & c^{2213} & c^{3313} & c^{1213} & c^{2313} & c^{1313} \end{bmatrix}$$

which is the *elasticity matrix*.

Figure 4.2: *Elasticity matrix in COMSOL Multiphysics™ Structural Mechanics module*

In the case considered the matrix of elasticity needs to be expanded to a 9x9 matrix with all the components. The reason for this is that the elasticity matrix is non-symmetric in this case. Below is an illustration of a general 9x9 elasticity matrix and how it looks for the case considered.

$$C = \begin{bmatrix} c^{1111} & c^{1122} & c^{1133} & c^{1112} & c^{1123} & c^{1113} & c^{1121} & c^{1131} & c^{1132} \\ c^{2211} & c^{2222} & c^{2233} & c^{2212} & c^{2223} & c^{2213} & c^{2221} & c^{2231} & c^{2232} \\ c^{3311} & c^{3322} & c^{3333} & c^{3312} & c^{3323} & c^{3313} & c^{3321} & c^{3331} & c^{3332} \\ c^{1211} & c^{1222} & c^{1233} & c^{1212} & c^{1223} & c^{1213} & c^{1221} & c^{1231} & c^{1232} \\ c^{2311} & c^{2322} & c^{2333} & c^{2312} & c^{2323} & c^{2313} & c^{2321} & c^{2331} & c^{2332} \\ c^{1311} & c^{1322} & c^{1333} & c^{1312} & c^{1323} & c^{1313} & c^{1321} & c^{1331} & c^{1332} \\ c^{2111} & c^{2122} & c^{2133} & c^{2112} & c^{2123} & c^{2113} & c^{2121} & c^{2131} & c^{2132} \\ c^{3111} & c^{3122} & c^{3133} & c^{3112} & c^{3123} & c^{3113} & c^{3121} & c^{3131} & c^{3132} \\ c^{3211} & c^{3222} & c^{3233} & c^{3212} & c^{3223} & c^{3213} & c^{3221} & c^{3231} & c^{3232} \end{bmatrix} = \begin{bmatrix} c^{1111} & c^{1122} & 0 & 0 & 0 & 0 & 0 & 0 & 0 \\ c^{2211} & c^{2222} & 0 & 0 & 0 & 0 & 0 & 0 & 0 \\ 0 & 0 & 0 & 0 & 0 & 0 & 0 & 0 & 0 \\ 0 & 0 & 0 & c^{1212} & 0 & 0 & c^{1221} & 0 & 0 \\ 0 & 0 & 0 & 0 & 0 & 0 & 0 & 0 & 0 \\ 0 & 0 & 0 & 0 & 0 & 0 & 0 & 0 & 0 \\ 0 & 0 & 0 & c^{2112} & 0 & 0 & c^{2121} & 0 & 0 \\ 0 & 0 & 0 & 0 & 0 & 0 & 0 & 0 & 0 \\ 0 & 0 & 0 & 0 & 0 & 0 & 0 & 0 & 0 \end{bmatrix}$$

This matrix is then implemented into COMSOL Multiphysics™ by a modification.

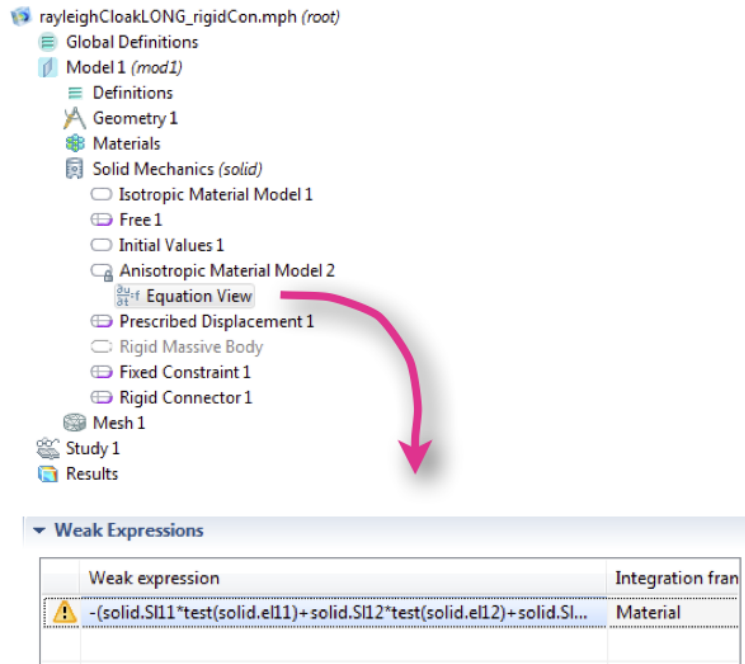


Figure 4.3: *Modifying module in COMSOL MultiphysicsTM*

The relevant module is based on weak form formulation, and may be modified to suit the problem on hand. In order to implement the non-symmetric 12 and 21 components, the weak formulation was modified in the Linear Elastic Material model, see Figure 4.3.

Name	Expression
C1111	$((\text{lambda0}+2*\text{mu0})*\text{fi}(\text{sys2.r}))/(\text{sys2.r}*\text{fip}(\text{sys2.r}))$
C2222	$((\text{lambda0}+2*\text{mu0})*\text{sys2.r}*\text{fip}(\text{sys2.r}))/\text{fi}(\text{sys2.r})$
C1122	lambda0
C2211	lambda0
C1221	mu0
C2112	mu0
C1212	$(\text{mu0}*\text{fi}(\text{sys2.r}))/(\text{sys2.r}*\text{fip}(\text{sys2.r}))$
C2121	$(\text{mu0}*\text{sys2.r}*\text{fip}(\text{sys2.r}))/\text{fi}(\text{sys2.r})$

Figure 4.4: *Modified stiffnesses.*

The non-zero components of the modified elasticity matrix that were used in the model for the anisotropic cloaking material is illustrated in Figure 4.4.

5 Results

In order to validate the model considered in the thesis work, first the results of the special case of cloaking transformation by Brun [7] are illustrated. Thereafter the model is simulated in COMSOL MultiphysicsTM and the results are presented.

5.1 Special case - Verification for bulk waves

In order to validate the model considered in the thesis work a comparison to Brun results is made. Here the elastic cloak is embedded in an isotropic elastic material with Lamé moduli $\lambda = 2.3Pa$ and $\mu = 1Pa$ and the density $\rho = 1m/s^2$, which corresponds to normalized parameters for fused silica. $r_0 = 0.2m$ and $r_1 = 0.4m$ can be used in the example as well as a harmonic concentrated force applied in x-direction with angular frequency $\omega = 40Hz$.

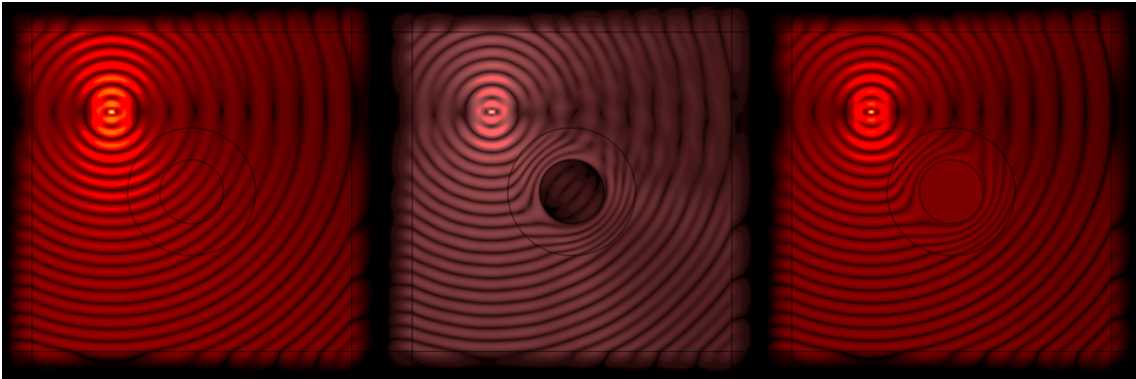


Figure 5.1: *Brun Cloak*

The three pictures in Figure 5.1 correspond to three different cases; from left, only homogeneous material, special case of cloaking transformation by Brun and finally an improvement of the model by Brun with a rigid body. In the first case, when only homogeneous material is applied, the re-routing of the waves does not occur at all, which is as predicted. Considering the Brun cloak, where the inner circular material is isotropic as the outer material, even though it has a cloaking effect a shadow is present, which should be minimized. A possible modification that can be made is to use a rigid body in the inner circle as in this thesis, this leads to a better cloaking with less shadow. A further comparison between the different cases can be seen in Figure 5.2 and Figure 5.3 which illustrate the displacement along a diagonal cut-through of the geometry in Figure 5.1.

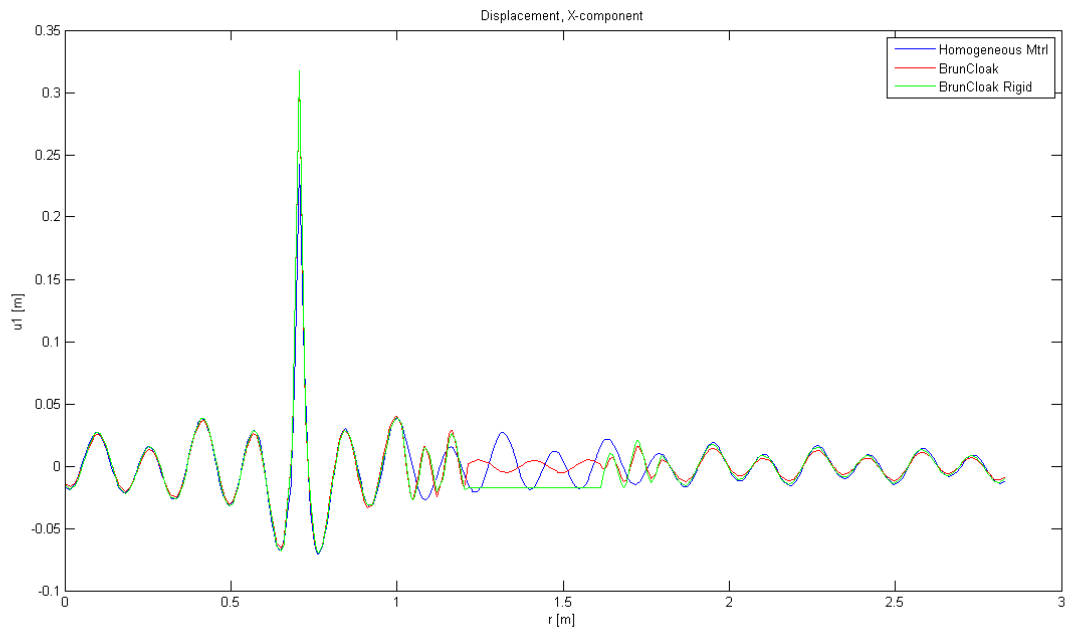


Figure 5.2: Cloak performance X-direction

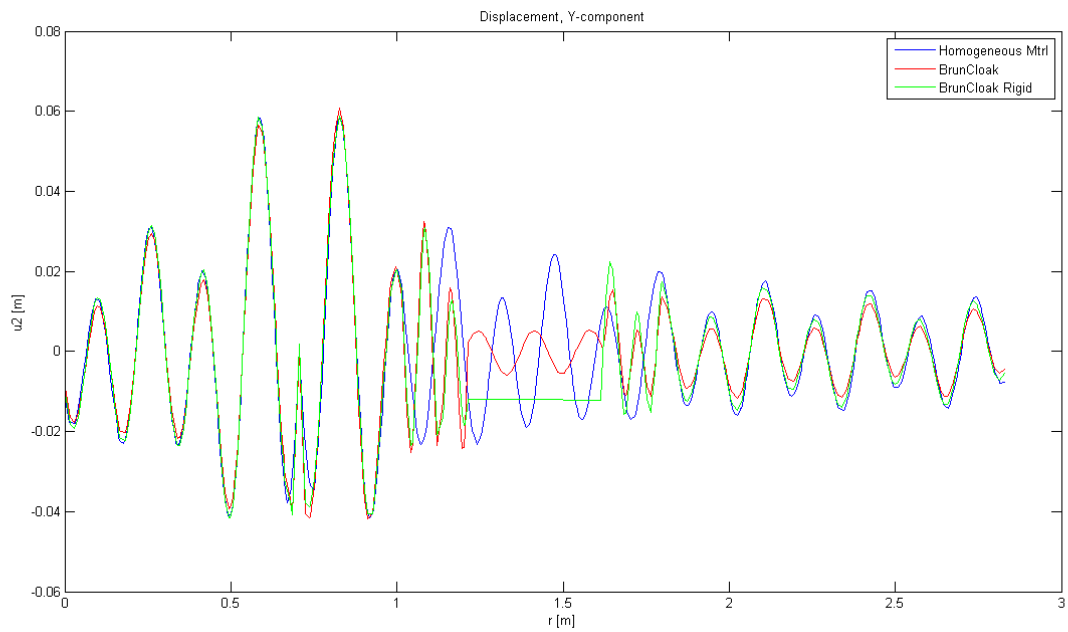


Figure 5.3: Cloak performance Y-direction

Comparing the three different cases we can clearly see that Brun cloak mimics the homogenous material very well. With a modification of the material inside the cloak to be a rigid body, the results are even better.

5.2 Considered case - Cloaking for surface waves

The results from the special case of cloaking transformation [7] have been reconstructed, the focus is shifted to the considered problem. Consider the geometry indicated in Figure 5.1, where a pipeline is partially buried in the ground.

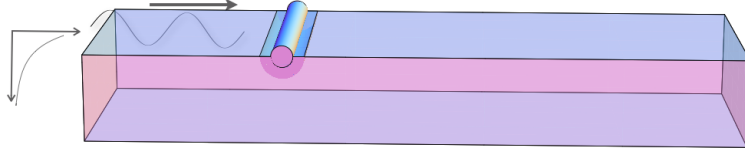


Figure 5.1: A light pipeline, partially buried in a homogeneous and isotropic ground.

We consider two types of support for the pipeline. First the layer between the soil and the pipeline is just made of the same homogeneous and isotropic material as the rest of the ground, and the pipeline is in ‘welded’ contact with the support. In the second case we consider the intermediate layer to be made of a micro-polar material which is graded so that it cloaks the pipeline. The diffeomorphism chosen only affects the radial coordinate r , measured from the rotational symmetry axis of the pipeline. We put $\psi(\mathbf{r}) = \phi(r)\mathbf{e}_r$, with $\phi(r)$ being an invertible map of $r_0 < r < r_1$ onto $0 < r < r_1$, where r_0 is the inner radius and r_1 the outer radius of the cloaking layer. Since we demand $\phi(r_1) = r_1$, the transformation (in 2D) must allow

$$\int_{r_0}^{r_1} \rho(r)rdr = \frac{1}{2}\rho_0r_1^2 \quad (5.2.1)$$

which constitutes a necessary condition on the density function. (Incidentally, this guarantees that the total mass of the cloak is finite, and in fact equal to the mass of the homogeneous half cylinder it mimics.) There are of course an infinity of transformations of this type, and we chose one of these, namely

$$\phi(r) = r_1 \sqrt{\frac{r^2 - r_0^2}{r_1^2 - r_0^2}} \quad (5.2.2)$$

5.2.1 Geometry

The geometry that was used needed to be elongated, in order to simulate uni-directional propagation of Rayleigh waves. In order to even better model the infinite medium around the model, perfectly matched layers (PML) were implemented.

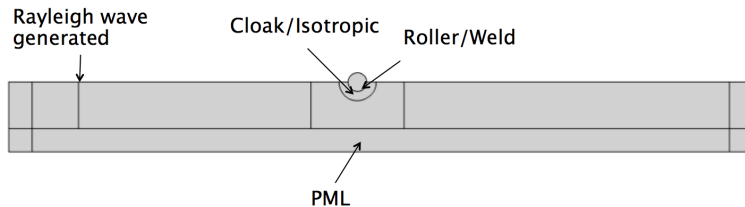


Figure 5.2: The geometry

Two different cases were simulated, one with a sliding, a.k.a. roller, boundary condition between the massive body and the cloak, and the other one with a welded contact and no cloaking material, *cf.* Figure 5.2.

5.2.2 Mesh

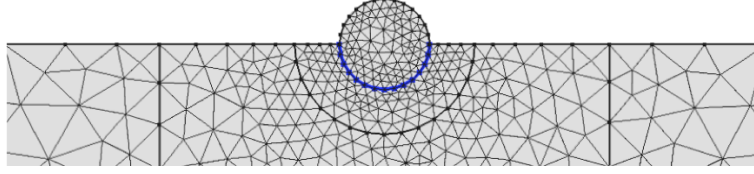


Figure 5.3: *The mesh*

The time step is a crucial part of the simulation procedure in COMSOL MultiphysicsTM. To illustrate this, values on ρ , μ , and ω have been used from the previous section. In order to obtain a suitable illustration, the time increment has to be within the following tolerance

$$\Delta t < \frac{L}{C_s} \quad (5.2.3)$$

where L is the mesh element size, $C_s = \sqrt{\mu/\rho} = 1$ m/s, is the shear wave speed and Δt is the time increment. The time increment will thus only depend on the element size: $\Delta t < L$. Rayleigh wave speed can then be approximated as shear wave speed and the equation still holds. In our model we used the time-dependent solver in order to see the effects of Rayleigh wave propagation. The simulation ended at 10s with a time-step of 0.1s which was chosen to be less than that corresponding to the element size, see Figure 5.3, and sufficiently small, balancing accuracy against computing time. By using smaller time-stepping we get better accuracy in the results, but the computation speed may be slow.

5.2.3 Simulation results

In addition to introducing the cloak, we decouple the pipeline further by allowing it to slide without friction on the cloaking layer.

In the simulations, the combined effect of the sliding BC and the cloak is to decrease the amplitude of the movement of the pipeline induced by the incident Rayleigh wave by at least five orders of magnitude.

In Figure 5.4 we see two snapshots as the (transient) Rayleigh wave impinges on the pipeline from the left in the picture.

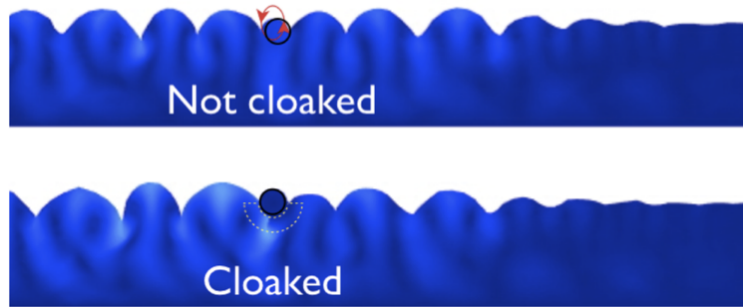


Figure 5.4: *Snapshots of transient Rayleigh wave incident upon an un-cloaked, welded, and a cloaked, sliding, pipeline, respectively. (Note that the scale of the displacement is immensely exaggerated, since we are actually in the linear regime.) The approximate path followed by the pipeline in the uncloaked case is indicated by an ellipse.*

In both cases the cylindrical pipeline rotates on a roughly elliptical path, counterclockwise, but the amplitude in the cloaked, sliding, case is so small that it cannot be discerned at this scale. From an animation of the movement, we find [7] that when the Rayleigh wave enters the cloaking layer, it essentially ‘dives’ under the pipeline and resurfaces behind the pipeline. In this way the cloak protects the pipeline from potential damage.

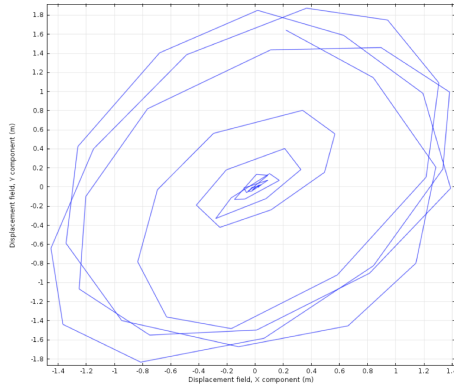


Figure 5.5: *Movement of pipeline in welded contact with homogenous material*

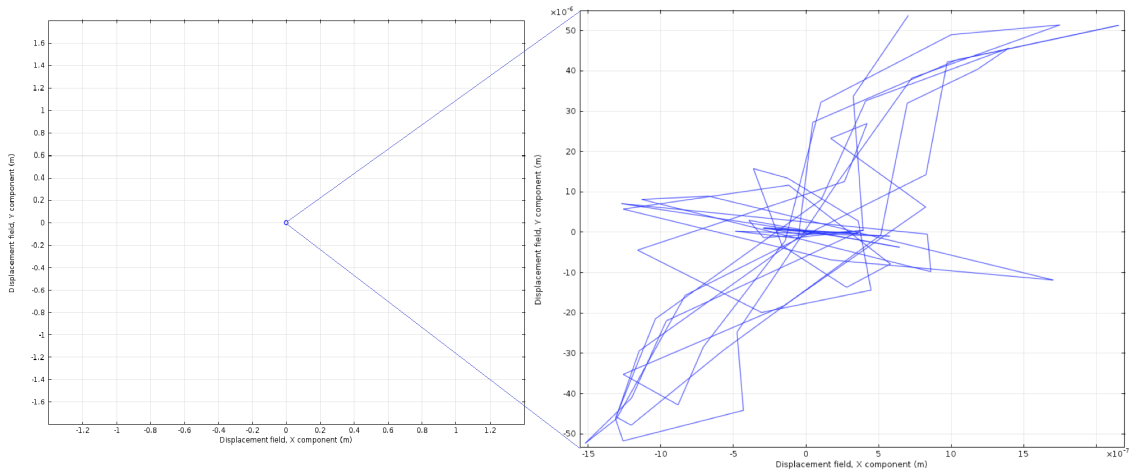


Figure 5.6: *Movement of pipeline rolling on a micropolar cloak*

Comparing the movements in the two cases, see Figure 5.5 and 5.6, we see that the cloak in conjunction with rolling (or sliding) boundary conditions decreases the induced oscillation of the pipeline with many orders of magnitude! Already the use of rolling contact in fact brings a considerable decrease of the induced movement. Notable is that the Rayleigh wave movement is elliptical and so is the movement of the pipeline. The difference is that the elliptical path taken by the pipeline is slightly rotated to the right compared to the Rayleigh wave motion. The reason for this effect is because of scattering, when the Rayleigh wave reaches the near side of the pipe a reflection occurs. Because of the reflection, the force on the far side is lower than the force on the near side, therefore the pipe generates a tilted elliptical rotation as can be seen.

6 Discussion

During the thesis a number of complications have been dealt with and solved in order to make us of the model described in Chapter 2-3. Because there are immense amount of possible transformations to transform the coordinates of a homogenous material on to a anisotropic (cloaking) material, a suitable transformation was therefore used as described in Chapter 5. Other diffeomorphism have not been tested, but there are future possibilities.

In order to simulate the different cases discussed, COMSOL MultiphysicsTM was chosen as the main software to use. The reason is that there are articles/papers published covering the same inverse problem area as considered in the thesis with good results, using the chosen software, COMSOL MultiphysicsTM[7]. In order to get an understanding of the software and how to implement the case of interest in the thesis, simulations from an already published article [7] were reconstructed. During the reconstruction it was noted that the original Structural Mechanics module in COMSOL MultiphysicsTM did not support the non-symmetric elasticity tensor \mathbf{C} (the anti-symmetry of the 12 and 21 components of the tensor). To overcome this obstacle it was made clear that COMSOL MultiphysicsTM is based on weak-form formulation and therefore could be modified to suite the problem on hand, see Chapter 4 for further details.

There are at least two different approaches when it comes to homogenization of different materials; first-order and second-order computational homogenization. However, in their standard format these techniques require that the elasticity tensor \mathbf{C} is symmetric. The material model considered in the thesis is based on the constitutive equations of micro-polar material which require that the elasticity tensor is non-minor symmetric in order to have the cloaking abilities. This is why first- and second-order computational homogenization schemes are not directly applicable and other homogenization techniques need to be investigated. In order to obtain improved results of the reconstruction some potential error sources were covered. Firstly, we had the modifications made to the software in order to implement the non-symmetric elasticity tensor. To guarantee that the modifications were made correct a comparison to the already existing results [7] was done. For the case in the thesis, a different transformation from the one in the mentioned article was used, and further confirmed working as the one from the article.

Furthermore, the finite element mesh size could be seen as an error source. The mesh should be "fine" enough to cover the effects of the Rayleigh wave and "course" enough to be effective and fast when running the simulation. Calculation of the velocity of the Rayleigh wave was done in Chapter 5 and thereafter a suitable time-step could be chosen based on the time step formula in the same chapter. When it comes to the transformation from a homogeneous material into an anisotropic material, the calculations where confirmed analytically by the use of Mathematica. Finally, there are a set of approximations made in the model. In order to model the rigid body, the density should be infinitely small while the Lamé parameters should be infinitely large. This is of course not possible to implement into the software and the parameters were set much smaller/larger than the surrounding material. The components of the elasticity tensor of the cloaking material, anisotropic material, should also be infinitely small/large and were set to be much smaller/larger than the surrounding isotropic material.

The results obtained from this thesis touches upon sustainable development in the way that it takes material aspects for different areas into consideration. For instance, if the described cloaking material is developed and manufactured in the future, then the possibility of prolonging infrastructural life can be a possibility. The prolongation will be obtained by protection of the specific infrastructure from potentially harmful, seismic waves and vibrations that can cause destruction otherwise.

7 Conclusions

Summing up, it can be concluded that elastodynamic cloaking from Rayleigh waves is theoretically possible, using a certain limiting type of such materials. However, this should come as no great surprise, as it has already been shown that cloaking against bulk waves is possible in that manner. In fact, the Rayleigh wave at a horizontal plane may be represented as a linear combination of such waves, albeit with imaginary wave numbers in the vertical direction. COMSOL MultiphysicsTM proved to be useful, after some modification, to perform the modeling of this type of cloak.

Future work may involve development of different homogenization techniques in order to model the substructure of the micro-polar material, which returns the desired cloaking properties on the macroscale. A study of several alternative approaches to minimize movements induced by elastic surface waves may be involved by using other material models, e.g. fiber-reinforced materials, porous medium. Finally, it is of interest to see if the material can be constructed and tested in real-life.

References

- [1] B. Banerjee. “An Introduction to Metamaterials and Waves in Composites”. In: *CRC Press* (2011).
- [2] K. R. F. Larsson and F. Su. “Variationally consistent computational homogenization of transient heat flow”. In: *International Journal for Numerical Methods in Engineering* 81 (2009).
- [3] M. B. G. W. Milton and J. R. Willis. “On cloaking for elasticity and physical equations with a transformation invariant form”. In: *New Journal of Physics* 8 (2006).
- [4] K. R. H. Johansson and F. Larsson. “Calibration of a Nonlinear Elastic Composite With Goal-Oriented Error Control”. In: *International Journal for Multiscale Computational Engineering* (2005).
- [5] F. Larsson and K. Runesson. “Rve computations with error control and adaptivity: the power of duality”. In: *Computational Mechanics* 39 (2007).
- [6] R. Larsson and S. Diebels. “A second-order homogenization procedure for multi-scale analysis based on micropolar kinematics”. In: *International Journal for Numerical Methods in Engineering* 69 (2006).
- [7] S. G. M. Brun and A. B. Movchan. “Achieving control of in plane elastic waves”. In: *Applied Physics Letters* (2009).
- [8] S. G. M. Farhat and S. Enoch. “Ultrabroadband elastic cloaking in thin plates”. In: *Physical Review Letters* 103 (2009).
- [9] V. M. Geers and W. Brekelmans. “Multi-scale computational homogenization: trends and challenges”. In: *Jnl. Comp. Appl. Math* (2010).
- [10] G. W. Milton. “New metamaterials with macroscopic behavior outside that of continuum elastodynamics”. In: *New Journal of Physics* 9 (2007).
- [11] M. R. N. S. Ottosen and C. Ljung. “Rayleigh waves obtained by the indeterminate couple-stress theory”. In: *Eur. J. Mech. A Solids* 19 (2000).
- [12] S. Nemat-Nasser and M. Hori. “Micromechanics: Overall properties of heterogeneous materials”. In: *Elsevier* (1993).
- [13] A. Norris and A. L. Shuvalov. “Elastic cloaking theory”. In: *Special Issue on Cloaking* 48 (2011).
- [14] A. N. Norris. “Acoustic cloaking theory”. In: *Proceedings of the Royal Society A* (2008).
- [15] P. Olsson. “Non-uniqueness of time-domain reflection from 3D planar elastic layers”. In: *Special Issue on Cloaking* 48 (2011).
- [16] P. Olsson and D. J. N. Wall. “Partial elastodynamic cloaking by means of fiber-reinforced composites”. In: *Inverse Problems* 27 (2011).
- [17] W. Pabst. “Micropolar materials”. In: *Ceramics - Silikáty* ().
- [18] O. Sigmund. “Tailoring materials with prescribed elastic properties”. In: *Mech. Mater.* 20 (1995).